




Functionalized mesoporous silica liquid crystal epoxy resin composite: an ideal low-dielectric hydrophobic material

Zhiqiang Feng^{1,3,5}, Xiaohong Liu^{3,5}, Wenchao Zhang^{2,4}, Juanjuan Zeng^{2,4}, Jiaming Liu^{1,3}, Bifang Chen^{1,5}, Jiaming Lin^{1,3}, Liqin Tan^{1,5}, and Liyan Liang^{1,2,3,4,*} 

¹Guangzhou Institute of Chemistry, Chinese Academy of Sciences, Guangzhou 510650, People's Republic of China

²Guangzhou Chemical Grouting Engineering Co., Ltd, Chinese Academy of Sciences, Guangzhou 510650, People's Republic of China

³CAS Engineering Laboratory for Special Fine Chemicals, Guangzhou 510650, People's Republic of China

⁴CASH GCC Shaoguan Research Institute of Advanced Materials, Nanxiong 512400, People's Republic of China

⁵University of Chinese Academy of Sciences, Beijing 100049, People's Republic of China

Received: 20 July 2021

Accepted: 24 October 2021

Published online:

3 January 2022

© The Author(s), under exclusive licence to Springer Science+Business Media, LLC, part of Springer Nature 2021

ABSTRACT

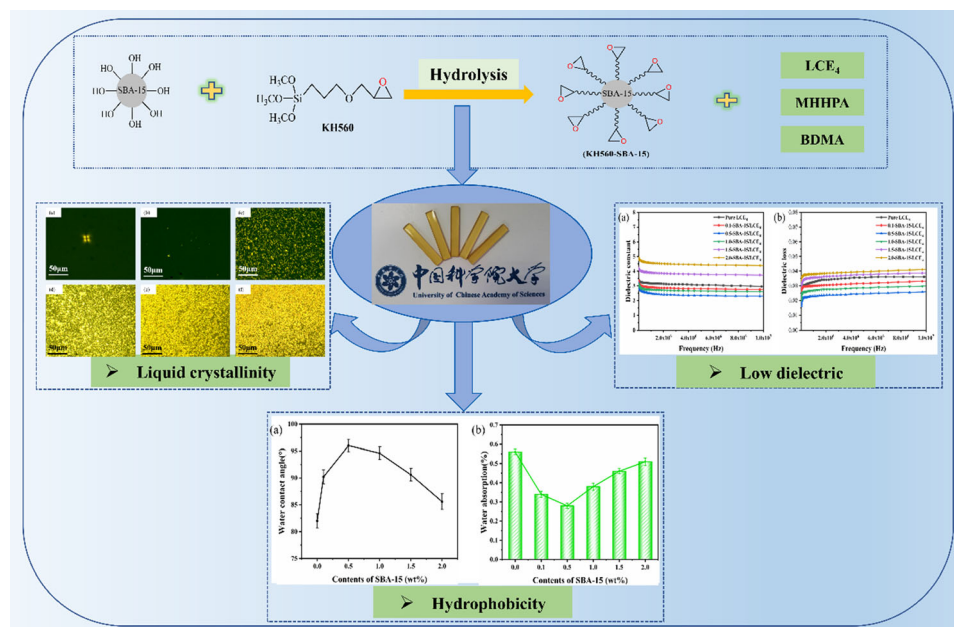
The field of microelectronic devices and 5G communication has an increasing demand for polymer composites with low dielectric constant, low dielectric loss, and good hydrophobicity. However, traditional polymer composites cannot simultaneously satisfy them, which severely hinders their application. In this work, a liquid crystal epoxy resin (LCE₄) consisted of a flexible chain and rigid mesogenic unit was prepared and cured with methylhexahydrophthalic anhydride (MHHPA). And the mechanism of the curing reaction and the phase structure of the liquid crystal epoxy resins were investigated. In addition, dielectric hydrophobic liquid crystal epoxy nanometer composite materials were successfully prepared with functionalized mesoporous silica (SBA-15) as a filler. The results showed that pure LCE₄ exhibited excellent dielectric properties and thermal stability. Compared with pure LCE₄, the composite material for SBA-15 modified with KH560 displayed lower dielectric constant, lower dielectric loss, higher glass transition temperature, and better hydrophobicity. For example, with a 0.5 wt% SBA-15, the dielectric constant and dielectric loss of the composite material were as low as (2.35, 0.025) compared with pure LCE₄ (3.25, 0.036) that was reduced by 24.7% and 31%. In addition, the glass transition temperature and water contact angle are increased by 16 °C and 14°, respectively. Composites also showed good thermal stability and mechanical properties. The reasons may mainly be derived from the internal structure of LCE₄,

Handling Editor: Maude Jimenez.

Address correspondence to E-mail: lyliang@gic.ac.cn

the effective modification of mesoporous SBA-15 by KH560, and the excellent dispersion of organic and inorganic phases.

GRAPHICAL ABSTRACT



Introduction

With the rapid development of 5G communication technology and the continuous miniaturization and integration of electronic equipment, higher and stricter requirements are put forward for the performance, reliability, and processing technology of advanced electronic packaging materials [1–6]. Microelectronic device packaging materials required low dielectric constant, dielectric loss, easy processing, and excellent hydrophobicity [7–10]. However, most polymers and composites can achieve some of the properties mentioned above [11] but still have high dielectric constant and poor hydrophobicity. Therefore, research on materials with excellent dielectric properties and hydrophobicity is imminent and has become a research hotspot of functional polymer composites [12–16]. As we all know, epoxy resin has a wide range of applications for the fields of coatings, composites, construction, electronics, and

electrical due to its excellent comprehensive properties and broad applicability [17–20]. However, due to the relatively high dielectric constant and dielectric loss, some applications are limited.

Previous studies reported that by introducing structurally ordered mesogenic units into the polymer matrix (the mesogenic unit is the rigid rod part of the liquid crystal epoxy molecule) and then induced by the curing agent to form a tight chemical cross-linked network [21]. Compared with ordinary epoxy resins, liquid crystal epoxy resin (LCE) has more evident advantages in electronic packaging materials, electronic and electrical applications. It is characterized by better thermal stability, mechanical properties, dielectric properties, and hydrophobicity [22–25]. In recent years, the application of liquid crystal epoxy resin in electronic packaging and electronic and electrical materials has gradually attracted people's attention [26–29]. Owing to its orderly structure and highly cross-linked network characteristics, it hinders the movement of molecules in an

external alternating electric field. At the same time, it also contains many low-polarity groups (C–C, C–H, C–O), which is highly conducive to the preparation of low-dielectric materials.

In addition, the most effective way to prepare low dielectric constant materials is to introduce pore structure into the material to increase its porosity. Owing to the existence of the pore structure, part of the air can be introduced into the pores (the dielectric constant of air is 1), thereby significantly reducing the dielectric constant of the material [30–32]. In general, introducing the pore structure into the material is achieved through a foaming agent. The pore size obtained by this method is not uniform, and the thermal and mechanical properties of the prepared composites are easily deteriorated [33, 34]. Many studies have shown that the pore size of inorganic nanoparticles with microporous and mesoporous structures is uniform, and the introduction to an ordered network structure can improve the thermal and mechanical properties of the material [35–38]. Among them, mesoporous silica (SBA-15) has a wide range of applications because of its uniform pore size, good thermal stability, and biocompatibility, and its surface is easily chemically modified [39, 40]. According to reports, mesoporous SBA-15 has a low dielectric constant, and the texture is chemically modifiable [41, 42]; its hydrophilic surface groups can be changed into hydrophobic groups of modification. The mesoporous SBA-15, after surface modification, is expected to be suitable for preparing polymer composites with excellent dielectric properties and good hydrophobicity.

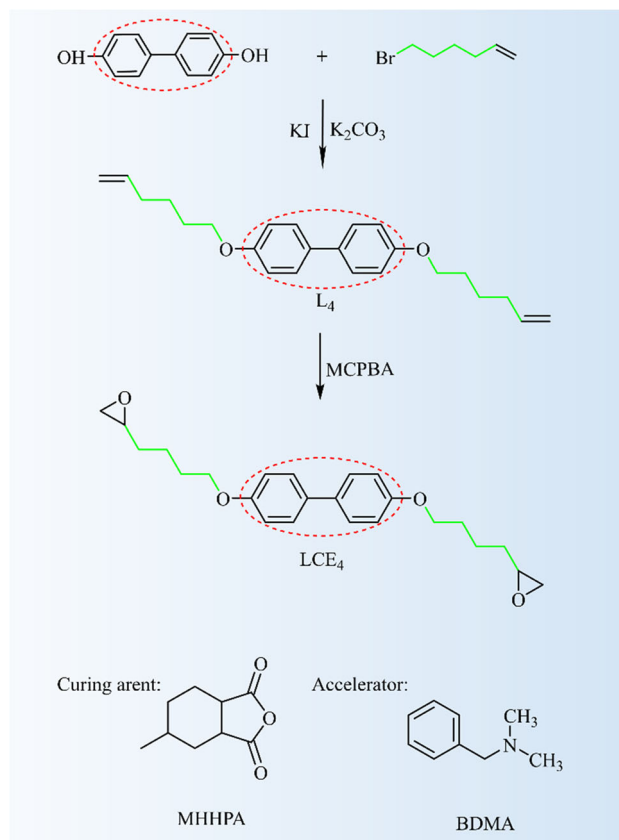
This work reports a method for preparing organic–inorganic nanocomposites by mixing liquid crystal epoxy resin (LCE_4) with surface-functionalized mesoporous silica (SBA-15). First, LCE_4 with the flexible chain was synthesized by a two-step synthesis method, and its structure and properties were characterized. Secondly, the surface functionalization of mesoporous SBA-15 was carried out synchronously by γ -glycidoxypropyltrimethoxysilane (KH560) and then uniformly dispersed in the liquid crystal epoxy resin as a low dielectric hydrophobic filler. Finally, corresponding SBA-15/ LCE_4 composites were prepared by in situ polymerization. The effects of the LCE_4 system and different mass fractions of surface-functionalized mesoporous SBA-15 on the dielectric properties, thermal properties,

mechanical properties, and hydrophobicity of SBA-15/ LCE_4 composites were systematically discussed.

Materials and methods

Materials

4,4'-Dihydroxydiphenyl (97%), 6-bromo-1-hexene (95%), potassium carbonate (99%), potassium iodide (99%), 3-chloroperoxybenzoic acid (MCPBA, 85%), methylhexahydrophthalic anhydride (MHHPA, 95%), N,N-dimethylbenzylamine (BDMA, 99%) were purchased from Aladdin; mesoporous silica (SBA-15, 95%) was purchased from Shanghai Yuanye Biotechnology Co., Ltd; γ -glycidoxypropyltrimethoxysilane (KH560, 98%) was from Nanjing Shuguang Chemical Group Co., Ltd; N,N-dimethylformamide (99.5%), dichloromethane (99.5%), ethanol anhydrous (99.7%), and acetone were provided by Guangzhou reagent factory; all



Scheme 1 The synthesis process of liquid crystal epoxy resin and the chemical structure formulas of MHHPA and BDMA.

chemicals were used as they were, and no further purification was required.

Synthesis of liquid crystal epoxy (LCE)

The liquid crystal epoxy resin was prepared by a two-step synthesis method as shown in Scheme 1

Preparation of 4, 4'-bis(5-propenyloxy) biphenyl (L_4)

The 4,4'-dihydroxydiphenyl (6 g, 0.032 mol) was dissolved in 150 mL N, N-dimethylformamide, 6-bromo-1-hexene (11 mL, 0.082 mol) was added, potassium carbonate (8.83 g, 0.064 mol) and potassium iodide (0.5 g, 0.003 mol) were mixed well and refluxed at 80 °C under nitrogen atmosphere for 24 h. The mixed solution was evaporated under reduced pressure, filtered, washed, and dried to obtain white powdery crystals, and the yield was 88% (9.8 g), named L_4 .

^1H NMR (400 MHz, CDCl_3 , ppm): 7.48 (d, 2H, Ar-H), 6.96 (d, 2H, Ar-H), 5.81 (m, 1H, $\text{CH}=\text{CH}_2$), 5.11–4.87 (d, 2H, $\text{CH}=\text{CH}_2$), 4.01 (t, 2H, OCH_2), 2.12 (m, 2H, $\text{CH}_2-\text{CH}=\text{CH}_2$), 1.76 (dd, 2H, OCH_2CH_2), 1.56 (m, 2H, CH_2).

^{13}C NMR (400 MHz, CDCl_3 , ppm): 158.22, 138.56, 133.42, 127.68, 115.59, 114.78, 67.89, 33.44, 28.78, 25.37.

Preparation of 4,4'-bis(2,3-epoxyhexyloxy) biphenyl (LCE_4)

The prepared L_4 (7.0 g, 0.02 mol) was dissolved in 180 mL of dichloromethane, added MCPBA (10.38 g, 0.06 mol) in batches, and reacted at 0 °C for 1 h. The reaction mixture was slowly heated to 40 °C and refluxed for 24 h. After the reaction, the crude product was filtered and then washed with 10% Na_2SO_3 solution, 5% NaHCO_3 solution, and deionized water successively. The organic phase was dried with anhydrous MgSO_4 , and dichloromethane was evaporated under reduced pressure to obtain light yellow solid. Crude product was repeatedly washed by anhydrous ethanol several times to get a white solid, and the yield was 84% (6.4 g) named LCE_4 . The epoxy value was determined by the hydrochloric acid-acetone method to be 0.52.

^1H NMR (400 MHz, CDCl_3 , ppm): 7.48 (d, 2H, Ar-H), 6.96 (d, 2H, Ar-H), 4.01 (t, 2H, OCH_2), 2.95 (s, 1H, CH_2 in epoxy), 2.78 (t, 1H, CH_2 in epoxy), 2.51 (dd,

1H, CH in epoxy), 1.85 (dd, 2H, OCH_2CH_2), 1.73–1.55 (m, 4H, CH_2CH_2).

^{13}C NMR (400 MHz, CDCl_3 , ppm): 158.14, 133.45, 127.69, 114.76, 67.74, 52.17, 47.02, 32.21, 29.10, 22.68.

The curing process of $\text{LCE}_4/\text{MHHPA}$

LCE_4 (5 g, 0.013 mol) was dissolved in 30 mL of acetone, and MHHPA (4.3 g, 0.026 mol) was added for sufficient mechanical stirring, then 1% (relative to the total mass of LCE_4 and MHHPA) BDMA as accelerator was added to the mixture, after mixing uniformly, evaporated under reduced pressure, and removed most of the solvent, then cast the mixture into the mold, and removed the solvent again under vacuum. Then, the temperature was raised, and the curing was carried out in stages at 110 °C for 3 h, 140 °C for 5 h, and 170 °C for 2 h.

Surface modification of SBA-15 and preparation of SBA-15/ LCE_4 composite

Before surface modification, the mesoporous silica was placed in a vacuum drying oven at 200 °C for 24 h; then, 2 g of activated SBA-15 was dispersed in 30 mL of toluene at room temperature ultrasonically and 1 g of silane coupling agent dropwise and continue ultrasonic dispersion for 1 h. Subsequently, the mixed solution was heated to 80 °C and refluxed for 6 h. After the reaction, the hybrid solution was suction-filtered and washed with toluene several times; finally, silane coupling agent-modified SBA-15 nanoparticles were obtained by drying in a vacuum drying oven. Figure 1 shows a schematic diagram of the modification process of mesoporous SBA-15.

The SBA-15/ LCE_4 composite was prepared by in situ polymerization. First, under the cutting-edge ultrasonic treatment, the stoichiometric ratio of LCE_4 , KH560-SBA-15, MHHPA, and BDMA (Table 1) was ultrasonically dispersed in toluene for 1.5 h. Then, the mixture was mixed with a Thinky Mixer (ARE250. Thinky) at 5000r/min stir at a rate of 1 h; after removing most of the solvent, we cast the mixture into a mold and removed the solvent again under vacuum. Then, the temperature was raised, and the curing was carried out in stages at 110 °C for 3 h, 140 °C for 5 h, and 170 °C for 2 h. Figure 1 shows the schematic diagram of the preparation process of the composites.

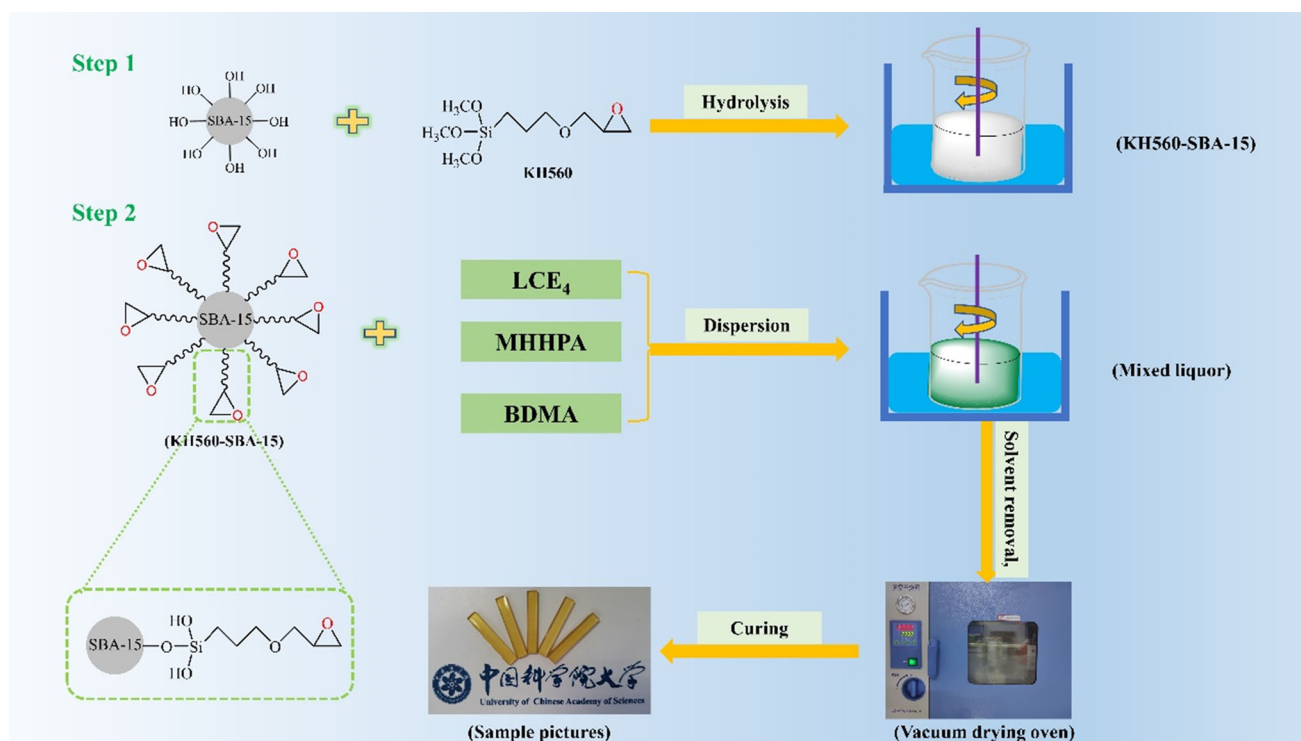


Figure 1 Schematic diagram of the surface modification of mesoporous SBA-15 and the preparation process of SBA-15/LCE₄ composites.

Table 1 The formula of liquid crystal epoxy resin composite

| Samples | LCE ₄ | KH560-SBA-15 /LCE ₄ composites(wt%) | | | | |
|---------------------|------------------|--|------|------|------|------|
| | | 0.1 | 0.5 | 1.0 | 1.5 | 2.0 |
| LCE ₄ /g | 10.0 | 10.0 | 10.0 | 10.0 | 10.0 | 10.0 |
| MHHPA/g | 8.8 | 8.8 | 8.8 | 8.8 | 8.8 | 8.8 |
| BDMA/g | 0.18 | 0.18 | 0.18 | 0.18 | 0.18 | 0.18 |
| KH560-SBA-15/g | 0.00 | 0.02 | 0.10 | 0.19 | 0.29 | 0.39 |

Characterization

Fourier transform infrared (FT-IR) spectroscopy was recorded on a German Bruker TENSOR 27 Fourier transform infrared spectrometer. The sample was mixed with KBr powder and pressed into a thin sheet. The measured spectrum range was 4000 to 400 cm⁻¹.

¹H NMR and ¹³C NMR spectra were recorded on a BRUKER AVANCE 400 spectrometer at room temperature, and the samples use CDCl₃ as a solvent.

A polarized light optical microscopy (Orthoplan, LEITZ, Germany with hot stage and temperature controller) was used to investigate the liquid crystal phase structure of the LCE₄. A small amount of the mixture of LCE₄, MHHPA, and BDMA was placed on

a glass slide, and then, the glass slide was placed on a hot stage to increase the temperature for curing, and the formation of the liquid crystal phase was studied.

The crystal structure of the cured resins was studied with wide-angle X-ray diffraction (WAXD). The diffraction patterns were recorded with a Rigaku diffractometer (D/MAX-1200), using monochromatic CuK α radiation (40 kV, 30 mA), and the scanning speed was 4°/min.

Fully automatic specific surface and porosity analyzer (BET, Mike 2460) were used to measure the nitrogen adsorption–desorption isotherm under a nitrogen atmosphere to obtain the nanopore size and specific surface area of the SBA-15 before and after modification were obtained. Before the test, the SBA-15 particles were preheated at 200 °C for 24 h.

Scanning electron microscope was used to observe the dispersibility of mesoporous SBA-15 in the composites.

A broadband dielectric spectrometer (Agilent 4294 A) was used to study the dielectric properties of the composites. The temperature was 25 °C, the frequency was 1 Hz to 1 MHz, and the sample size was 15 mm × 15 mm × 1 mm.

Differential scanning calorimetry (DSC) was examined via a TA Instrument NETZSCH DSC 200F3 to acquire glass transition (pure LCE₄ and SBA-15/LCE₄ composites). The measurements were heated from 25 to 250 °C with heating and cooling rates of 10 °C/min.

In the tensile mode, a dynamic thermomechanical analyzer (DMA, TA-Q800) was used to measure the dynamic thermomechanical properties. A sample with a size of 30 mm × 5 mm × 2 mm was scanned from 25 to 300 °C, the heating rate was 5 °C/min, the amplitude was 25 μm, and the frequency was 1 Hz.

The thermal stability of the composites was analyzed by a thermogravimetric analyzer (PE TGA8000, USA), and the test was conducted under nitrogen at a heating rate of 10 °C/min from 30 to 800 °C.

A universal testing machine (SHT5000 Shenzhen SANS testing machine) was used to conduct a tensile test on the composites, and the strain rate was tested at a rate of 3 mm/min.

A contact angle measuring instrument (Shanghai Zhongchen Digital Technology Equipment Co., Ltd. JC2000C type) was used to test the water contact angle of the composites.

The water absorption test was measured by the gravimetric method. A 15 mm × 15 mm × 1 mm sample was polished and dried in a vacuum oven at a constant temperature of 100 °C for one week. Then, it was soaked in deionized water. During the period, it was regularly eliminated from the water and wiped dry with a paper towel, then weighed it on an electronic balance of 1/10000, repeated the test for each sample three times, and calculated the average value.

Results and discussion

Synthesis and characterization of liquid crystal epoxy resin

Using 4,4'-dihydroxy biphenyl and 6-bromo-1-hexene as basic raw materials, a liquid crystal epoxy

resin matrix with flexible chains was prepared by a two-step synthesis method. Previous studies had reported that introducing a flexible spacer between the mesogenic nucleus and the reactive group could effectively reduce the melting point of LCE₄ and improve the stability of the mesophase [43–48]. It was worth mentioning that LCE₄ was prepared by epoxidation of olefins. Usually, the reaction took about a week at room temperature. In this study, two methods of ice-water bath and heating reflux were used in the preparation process. It only took a day to complete. FT-IR and NMR confirmed the successful preparation of a high-purity LCE₄ matrix. It could be obtained from Fig. 2a that the characteristic absorption peak of phenol –OH at 3362 cm⁻¹ disappeared before and after the 4,4'-dihydroxy biphenyl reaction, and new ones appeared 2939 cm⁻¹ and 2873 cm⁻¹. The absorption peak of –CH₂– and the appearance of a new absorption peak of –C=C– near 1642 cm⁻¹ could prove the formation of a further monomer L₄. In addition, the absorption peak of –C=C– to 1642 cm⁻¹ disappeared after the L₄ monomer was oxidized, which can be seen from Fig. 2b. Similarly, the chemical shift of H and the chemical change of C at each position in ¹H NMR and ¹³C NMR could be a one-to-one correspondence. The above results fully proved the successful preparation of the liquid crystal epoxy resin matrix (LCE₄).

The liquid crystal phase structure and curing mechanism of LCE₄/MHHPA

In this study, biphenyl is invoked as the liquid crystal rigid unit, combined with the appropriate flexible segment main chain, the perfect combination of rigidity and flexibility, giving LCE₄ unique liquid crystal properties [27]. POM and XRD analyzed the liquid crystal phase structure of LCE₄. The polarizing microscope images of cured LCE₄/MHHPA are shown in Fig. 3, and birefringence could be observed in all POM images. With the extension of curing time, the density of liquid crystal microdomains could be observed to increase gradually, indicating the existence of the liquid crystal phase, which was mainly due to the interaction between polarized light and the highly ordered structure of liquid crystal molecules. Figure 3f shows that the liquid crystal microdomain density is highest when the curing time was 180 min. At the same time, the “schlieren-like” structure could be observed in all POM images.

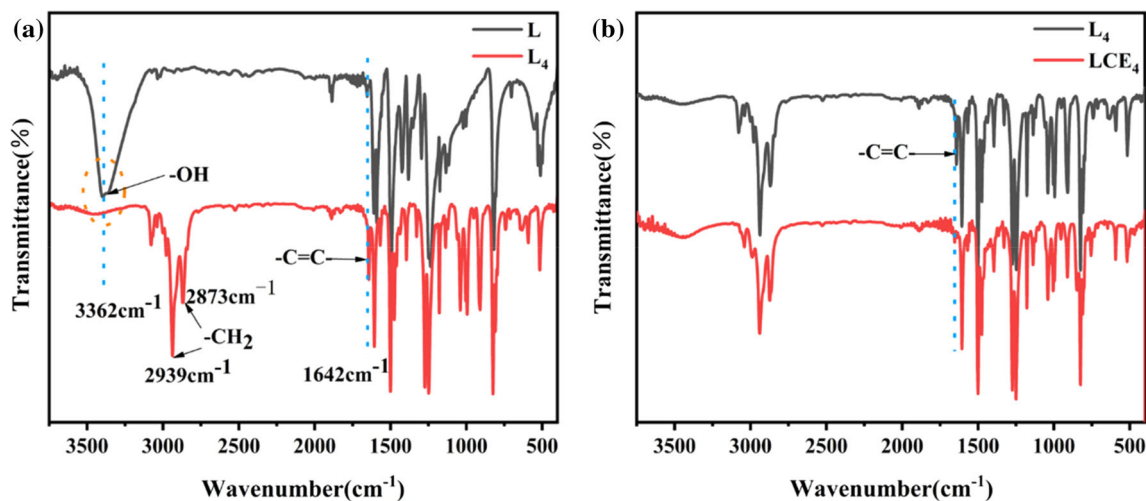


Figure 2 a IR spectra of 4,4'-dihydroxybiphenyl (L) and 4,4'-dihydroxybiphenyl derivatives (L₄), b 4,4'-dihydroxybiphenyl derivatives (L₄), and IR spectra of liquid crystal epoxy (LCE₄).

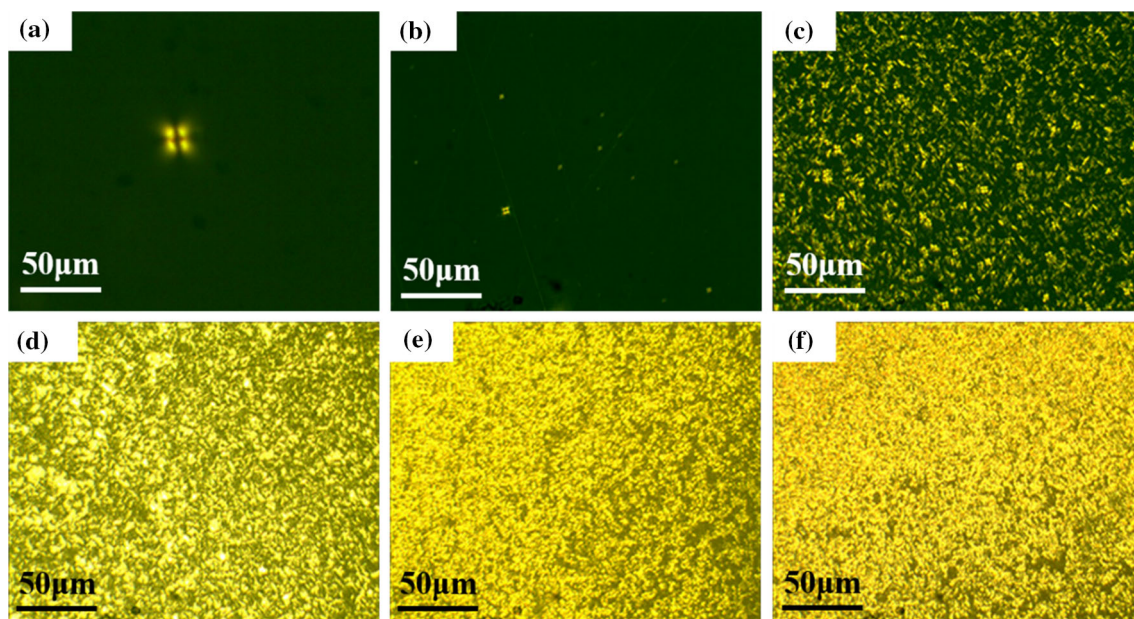


Figure 3 Polarized optical microscope (POM) images of LCE₄ cured by MHPA at 140 °C a 76 min, b 85 min, c 105 min, d 120 min, e 140 min, f 180 min.

The room-temperature wide-angle X-ray diffraction (WAXD) pattern of LCE₄ cured with MHPA at 140 °C is shown in Fig. 4b. It offered a robust and broad peak at $2\theta = 19.8^\circ$. The interplanar spacing $d = 4.49 \text{ \AA}$ was calculated by the Bragg equation. The diffraction peak at this position represented the nematic structure in LCE₄, corresponding to the lateral stacking of liquid crystal molecules [49]. The curing mechanism of LCE₄ is shown in Fig. 4a, including early linear chain extension, then branching, and finally cross-linking, which may have a

significant impact on the mesogenic orientation and structure of the liquid crystal epoxy resin [21]. Figure 4c shows the uniaxial orientation and nematic structure model of LCE₄, which was more helpful in understanding mesogenic units' direction. Based on the orderly and highly cross-linked characteristics of LCE₄, its application prospects will be more and more extensive.

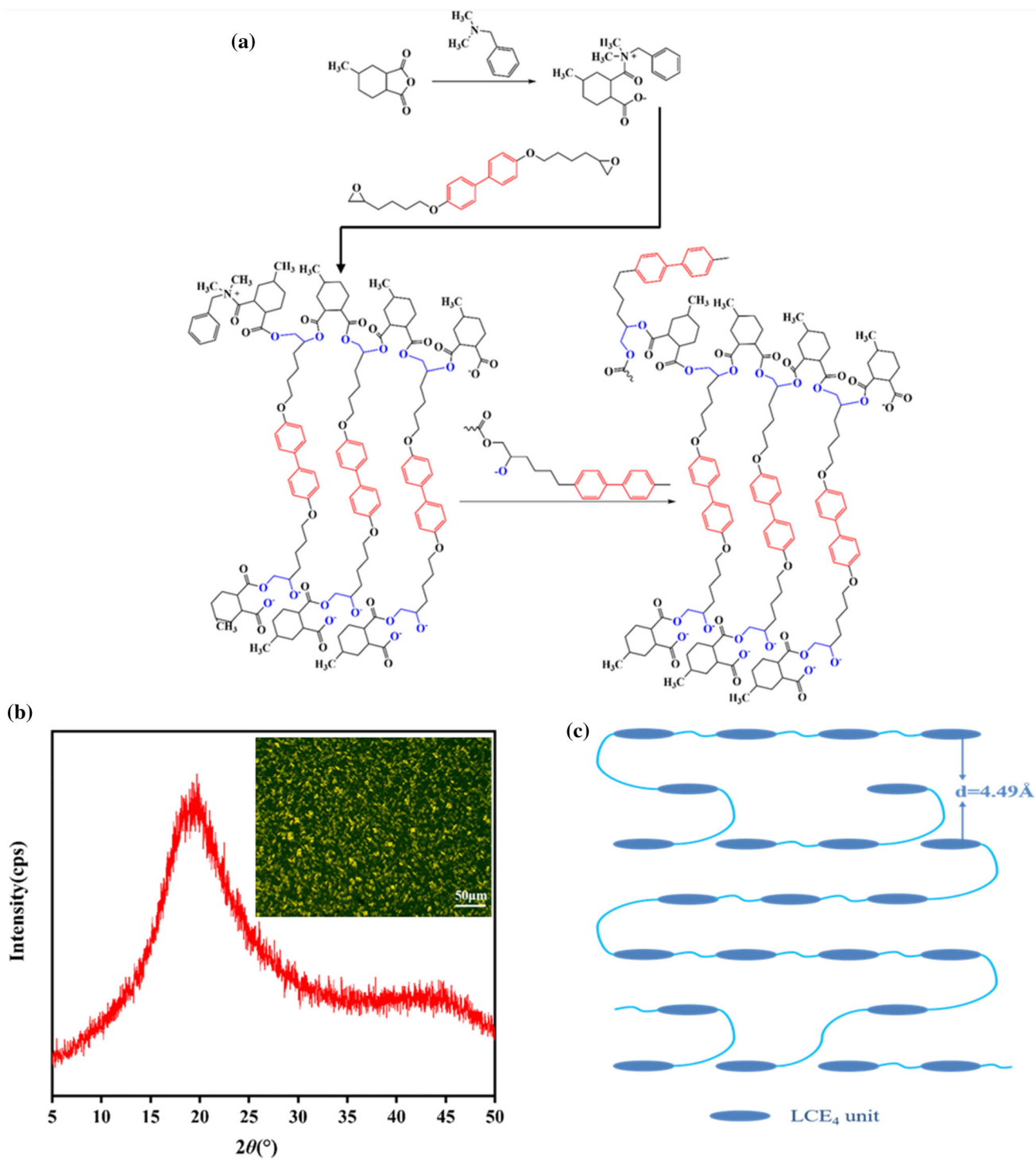


Figure 4 a The mechanism diagram of MHHPA curing LCE₄; b the room-temperature wide-angle X-ray diffraction (WAXD) diagram of LCE₄/MHHPA (the inset is the POM diagram); (c) the uniaxially oriented nematic phase structure of LCE₄/MHHPA model diagram.

Surface modification and characterization of mesoporous silica SBA-15

In this study, silane coupling agent KH560 was used to modify the surface of mesoporous SBA-15. The whole modification process was mainly divided into three steps: firstly, KH560 was hydrolyzed to produce Si–OH. Secondly, the Si–OH obtained by the hydrolysis and the –OH on the surface of the mesoporous SBA-15 was dehydrated to form an oligosiloxane. Finally, in the process of heating and dehydration, KH560 was combined with the character of mesoporous SBA-15 in the form of covalent bonds to complete the modification of mesoporous

SBA-15. Through chemical modification, the inorganic phase and the organic phase could be closely combined, which significantly enhanced the interfacial adhesion and improved the material's performance [50, 51]. Figure 5a shows the FTIR image of SBA-15 before and after modification. As could be seen from the figure, the characteristic absorption peak of mesoporous SBA-15 at 3425 cm^{-1} was the stretching vibration of Si–OH. After being modified by KH560, it widened, indicating that the Si–OH of SBA-15 nanoparticles reacts chemically with the alkoxy group in KH560. In addition, a new absorption peak appeared at 2912 cm^{-1} after modification of mesoporous SBA-15, which could be attributed to the

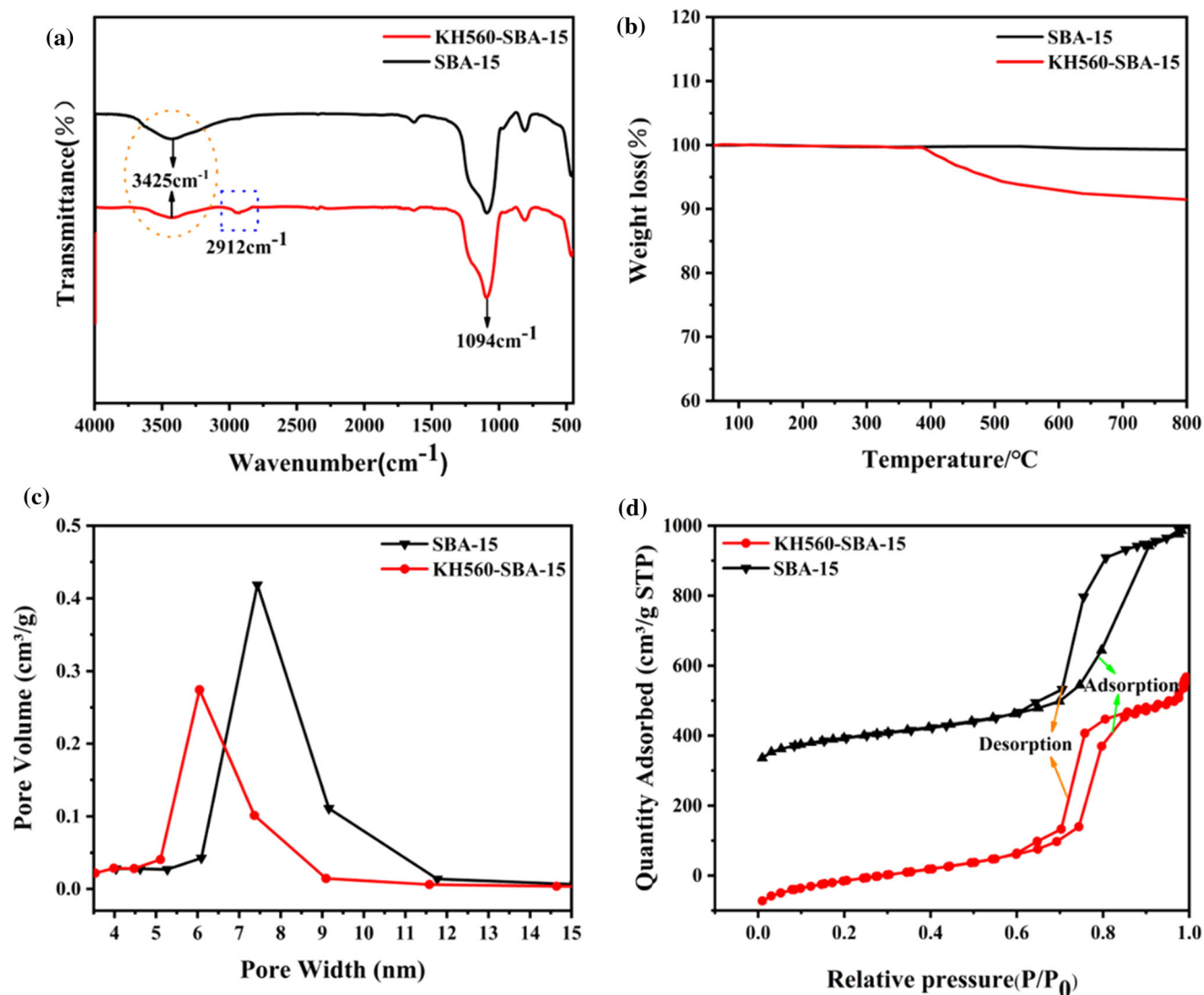


Figure 5 a The FTIR spectrum of SBA-15 before and after modification; b the TGA curve of SBA-15 before, and after modification; c the pore size distribution curve of SBA-15 before

and after modification; d the N₂ adsorption–desorption isotherm of SBA-15 before and after modification.

symmetric stretching vibration of $-\text{CH}_2-$. Surprisingly, however, no characteristic absorption peak was observed near 910 cm^{-1} for the epoxy group, possibly because the peak was covered by the strong absorption peak of the Si–O–Si antisymmetric stretching vibration at 1094 cm^{-1} . Figure 5b shows the thermal weight loss analysis of the SBA-15 nanoparticles before and after modification. It could be seen from the figure that the KH560-modified SBA-15 nanoparticles lose weight with the increased of temperature, and the weight loss rate was about 10%. In contrast, for the unmodified SBA-15 nanoparticles the mesoporous SBA-15 has not changed.

Figure 5c and d shows the BJH pore size distribution diagram and N_2 adsorption–desorption isotherm of mesoporous SBA-15 measured by the automatic specific surface area and porosity analyzer at 77 K. It could be seen from the figure that according to the classification of IUPAC mesoporous SBA-15 was behaved as a typical Langmuir IV isotherm with a clear H_1 hysteresis loop, indicating that it had the distinctive characteristics of a porous material. At the same time, it showed that the modification did not destroy its pore structure [52–54]. The changes in specific surface area, pore volume, and pore diameter of mesoporous SBA-15 before and after modification are shown in Table 2.

Through characterization methods such as FT-IR, TGA, BET, and BJH pore size distribution, it could be seen that the characteristic absorption peak, thermal weight loss, specific surface area, and pore size of Si–OH before and after the modification had changed significantly, indicating that KH560 affects mesoporous SBA-15 the modification of was triumphant.

Scanning electron microscope analysis of SBA-15/LCE₄ composite

The SEM images of LCE₄ and SBA-15/LCE₄ composites are illustrated in Fig. 6; the dispersibility of mesoporous SBA-15 in LCE₄ varies with the amount of addition. When the addition amount of mesoporous SBA-15 was 0.5 wt%, the dispersibility of

mesoporous SBA-15 and LCE₄ was good, and the result is shown in Fig. 6b. To further verify the excellent dispersibility of mesoporous SBA-15 and LCE₄ when the additional amount is 0.5 wt%, we had done EDS element analysis to illustrate it. The results are shown in Fig. 6d, e, and f; C, N, O, Si, and other elements all showed excellent dispersibility, which confirmed that the mesoporous SBA-15 and LCE₄ could be dispersed well. However, when the amount of mesoporous SBA-15 added was 2.0 wt%, there was some agglomeration of mesoporous SBA-15 in the composite, and the result is shown in Fig. 6c.

Dielectric properties and potential applications of SBA-15/LCE₄ composite

Low dielectric constant (Dk) and low dielectric loss (Df) epoxy resins and their composites are expected to play an increasingly important role in high-performance microelectronic devices and electronic packaging materials [21]. Therefore, new epoxy resins and composites with low dielectric constant and low dielectric loss were desirable. In this study, LCE₄ with a liquid crystal phase structure was prepared and used as a resin matrix to mix with modified mesoporous SBA-15 nanoparticles to prepare SBA-15/LCE₄ composites. The effect of the addition of mesoporous SBA-15 on the broadband dielectric properties of the composites is shown in Fig. 7.

Figure 7a and b shows the dielectric constant and dielectric loss of pure LCE₄ and the composites at 25 °C and frequencies from 1 Hz to 1 MHz. It can be seen from Fig. 7a and b that the dielectric constant and dielectric loss of pure LCE₄ at high frequency were 3.12 and 0.036. However, what is exciting is that the dielectric constant and dielectric loss of the composites gradually decrease with the increase in mesoporous SBA-15 content. When the addition amount of mesoporous SBA-15 was 0.5 wt%, the dielectric constant and dielectric loss of the composites were reduced to the lowest of about 2.35 and 0.025, which were decreased, respectively, compared with pure LCE₄ 24.7% and 31%. The reason for the significant decrease in the dielectric constant and

Table 2 Structural parameters of SBA-15 before and after modification

| Sample | Surface area (m^2/g) | Pore volume (cm^3/g) | Pore size (nm) |
|--------------|--|--|----------------|
| SBA-15 | 438.68 | 0.42 | 7.43 |
| KH560-SBA-15 | 312.44 | 0.27 | 6.05 |

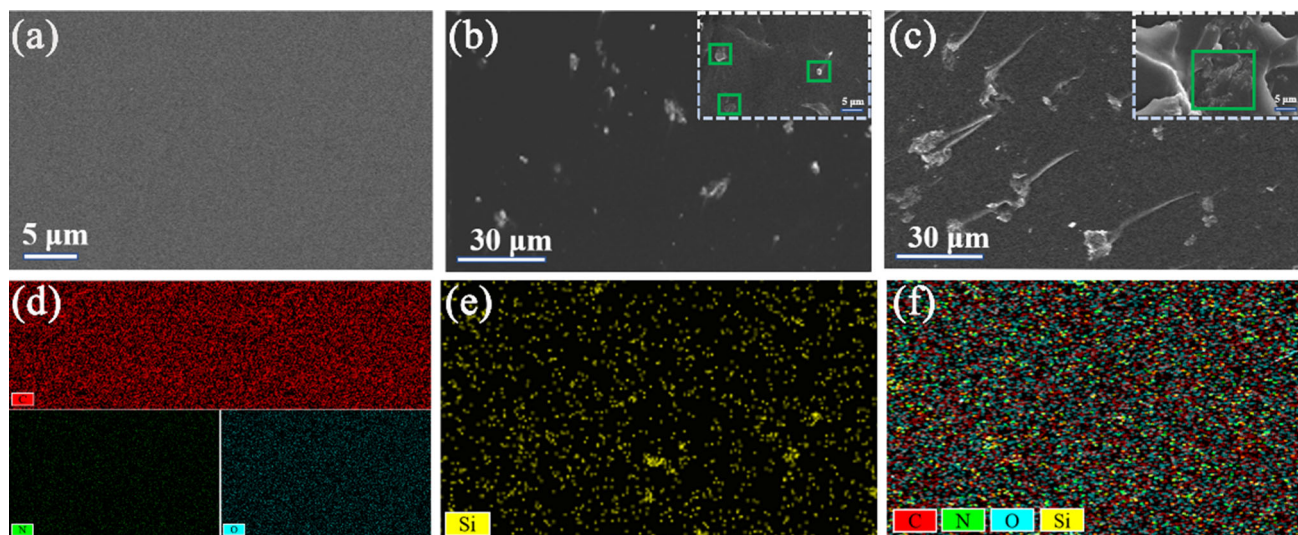


Figure 6 SEM images of SBA-15/LCE₄ composites: **a** pure LCE₄, **b** 0.5-SBA-15/LCE₄ when the additive amount was 0.5 wt%, **c** 2.0-SBA-15/LCE₄ when the additive amount was 2.0

wt%, **d**, **e**, **f** the EDS mapping result of the SBA-15/LCE₄ composite when the added amount was 0.5 wt%.

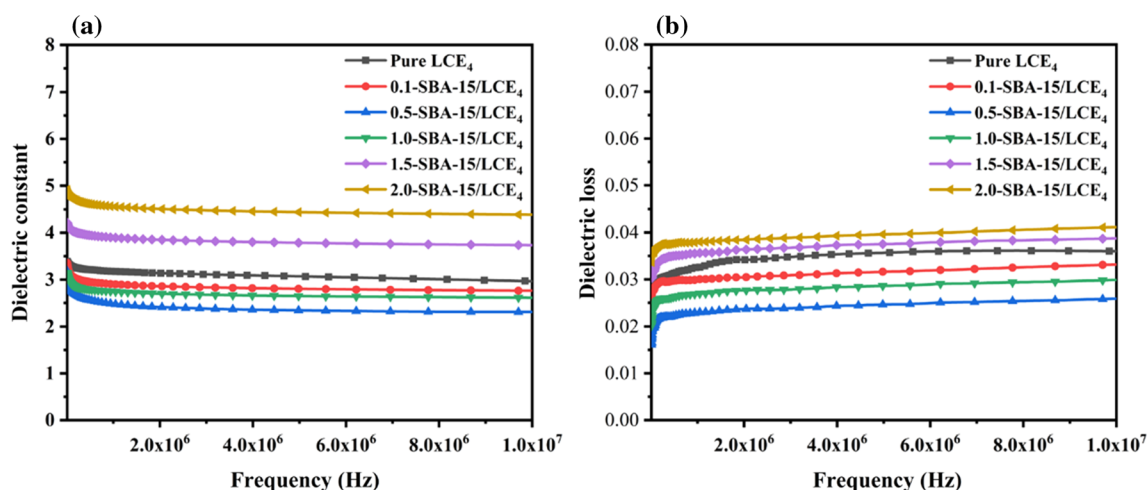


Figure 7 Dielectric constant diagrams **a** and dielectric loss diagram **b** of pure LCE₄ and SBA-15/LCE₄ composites.

dielectric loss was mainly due to the internal structure of LCE₄ and mesoporous SBA-15, as well as the dispersibility of mesoporous SBA-15 in composites.

The order of the orientation structure and the gradual increase in the packing density of the mesogenic unit in LCE₄ can effectively hinder the movement of molecular chains in the applied alternating electric field and reduce the dielectric constant and dielectric loss of the composite. In addition, since air has a low dielectric constant ($DK \approx 1$), air voids could be used to effectively reduce the dielectric constant of composites [55, 56]. In this work, the mesoporous SBA-15 has a large pore size. A part of

the air could be introduced into the mesopores during the preparation of the composites, thereby significantly reducing the dielectric constant. On the other hand, the dispersibility of the KH560-modified mesoporous SBA-15 in the composites was improved so that the inorganic phase and the organic phase were tightly combined, which enhanced the interfacial adhesion and further improved the dielectric performance. However, with increasing content of mesopore SBA-15, the dielectric constant and dielectric loss of the composite showed a growing trend when the additional amount was 1.5 wt% and 2.0 wt%, compared with that of pure LCE₄. The reason

could be that with the increase of mesoporous SBA-15 content, the dispersity of mesoporous SBA-15 in the composites gradually becomes worse and finally led to the agglomeration of mesoporous SBA-15 nanoparticles. Previous studies had shown that adding too much mesoporous SBA-15 will cause aggregation and poor dispersion, reducing the air volume [37]. Thus, the dielectric constant and dielectric loss are increased. Therefore, when the additional amount of mesoporous SBA-15 was 0.5 wt%, the effect of reducing the dielectric constant and the dielectric loss of the composites was significant.

Hydrophobicity of SBA-15/LCE₄ composite

The water contact angle of the prepared samples was measured to study the wettability of LCE₄ and SBA-15/LCE₄ composites. As shown in Fig. 8a, the contact angle of pure LCE₄ before adding SBA-15 was 82°. Meanwhile, compared with LCE₄, the composites were more hydrophobic. When the addition amount of SBA-15 was 0.1 wt%, 0.5 wt%, 1.0 wt%, 1.5 wt%, and 2.0 wt%, the water contact angles of the composite were 90.2°, 96°, 94.6°, 90.8°, 85.4°. This was primarily attributed to the hydrophilic group (–OH) on the surface of SBA-15 changed into the hydrophobic group after KH560 modification and the dispersion difference of SBA-15. As shown in Fig. 8a, with the increased of SBA-15 content, the water contact angle increased and then decreased. When the content of SBA-15 increased gradually, more SBA-15 aggregates would occur, leading to uneven dispersion of the composites, resulting in poor

compatibility and increased porosity between SBA-15 and LCE₄. Therefore, when the additional amount of SBA-15 exceeded 0.5 wt%, the water contact angle showed a decreasing trend.

Figure 8b shows the water absorption capacity of LCE₄ and the composites. In this study, the water absorption of the prepared sample was evaluated according to the weight difference between LCE₄ and the composites before and after soaking in deionized water. When different samples were soaked at room temperature for 24 h, the water absorption rate of pure LCE₄ was 0.54%, and the addition amount was 0.1 wt %, 0.5 wt %, 1.0 wt %, 1.5 wt %, and 2.0 wt %. The water absorption rates of the composites were 0.34%, 0.28%, 0.38%, 0.46%, and 0.51%, respectively. Under the condition of the low additional amount, SBA-15 and LCE₄ were uniformly distributed in the resin matrix to form a compact inorganic–organic hybrid composites, which hindered the penetration of oxygen and water to a certain extent water absorption. However, with the increase of SBA-15 addition, SBA-15 may aggregate and lead to more porosity. Therefore, low addition of SBA-15 could effectively reduce the water absorption of the composites.

Thermomechanical properties of SBA-15/LCE₄ composite

Glass transition temperature (T_g) is an important performance index used to measure thermoset materials. In this study, DSC and DMA were used to characterize the T_g of SBA-15/LCE₄ composites, as

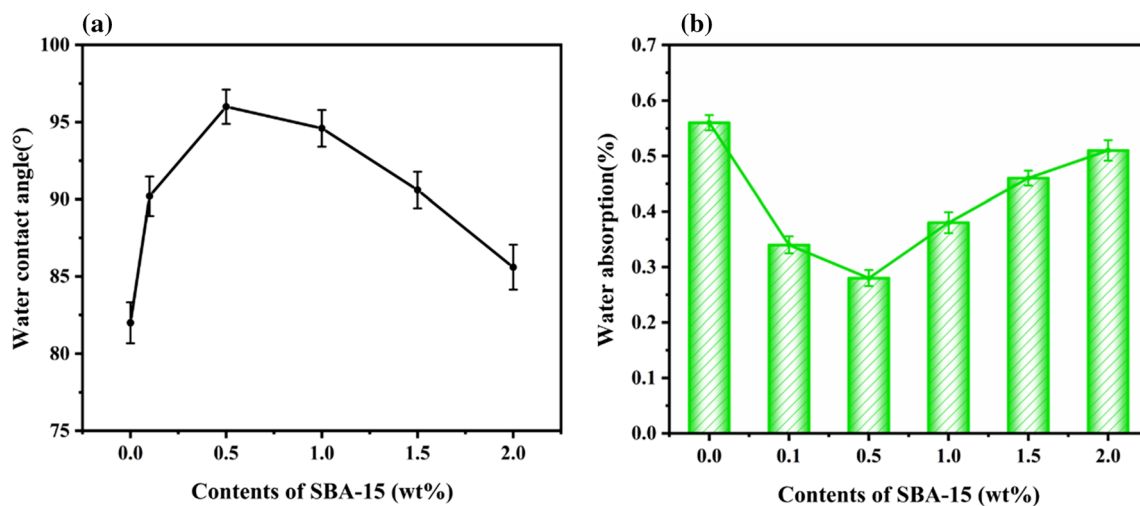


Figure 8 Water contact angle **a** and water absorption **b** of pure LCE₄ and SBA-15/LCE₄ composites.

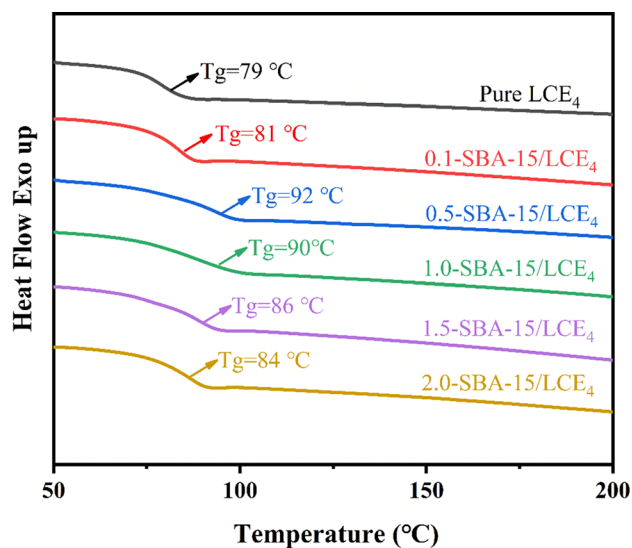


Figure 9 DSC curves of pure LCE₄ and SBA-15/LCE₄ composites.

shown in Fig. 9 and Fig. 10. The datum is summarized in Table 3. Obviously, with the addition of mesoporous SBA-15, the T_g of the composites changed. It was worth noting that the T_g of the composite increased by 16 °C compared with that of pure LCE₄ when the addition amount was 0.5 wt%, reaching a maximum of 101 °C. However, with the increase of SBA-15, the T_g of the composites decreased. The change of T_g of the composite was related to the pore structure of SBA-15 and the cross-link density of the composite. With the increase of mesoporous SBA-15 content, the cross-linking density of the composites increased slightly. (The cross-linking density is calculated by Eq. 1.) At the same time, the pore structure of SBA-15 restricted the movement of molecular chains, increasing T_g. In addition, the T_g of the composites was closely related to the dispersion between SBA-15 and LCE₄. Under the condition of

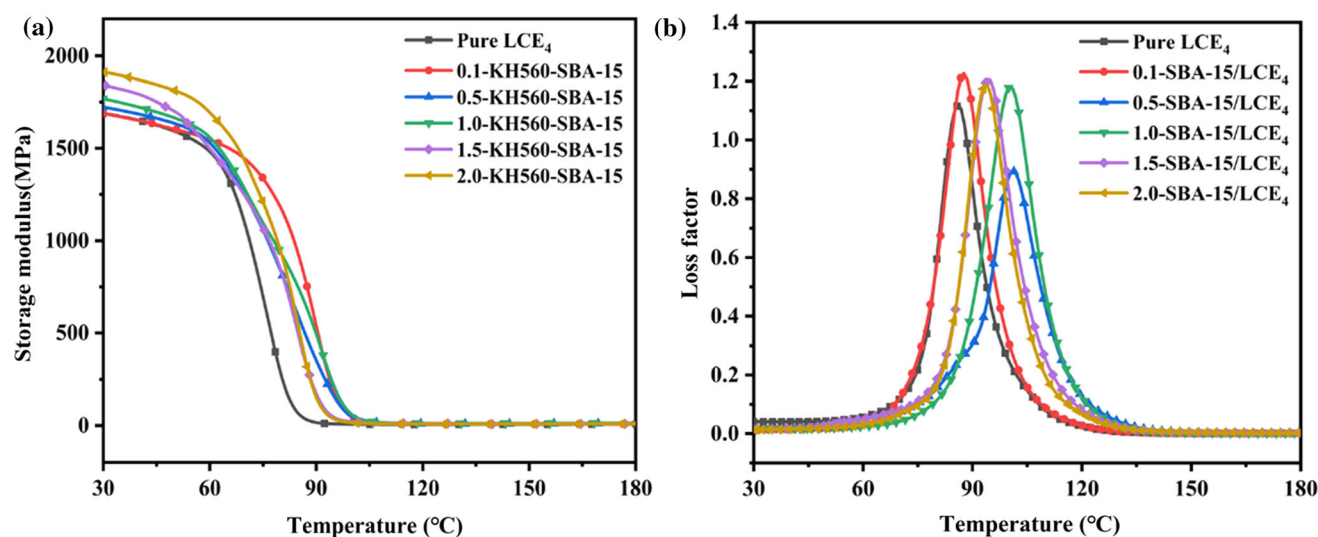


Figure 10 DMA curves of pure LCE₄ and SBA-15/LCE₄ composites.

Table 3 Glass transition temperature (T_g), storage modulus at T_g + 30 °C (*E'*_r), cross-link density (*v*_r) and thermal weight loss (T_{10%}, T_{50%}) of pure LCE₄ and SBA-15/LCE₄ composites

| Sample | T _g (°C) | | <i>E'</i> _r (MPa) | <i>v</i> _r (g mol ⁻¹) | T _{10%} (°C) | T _{50%} (°C) |
|-----------------------------|---------------------|-----|---------------------------------|---|--------------------------|--------------------------|
| | DSC | DMA | | | | |
| Pure LCE ₄ | 79 | 85 | 5.32 | 550 | 344 | 395 |
| 0.1-SBA-15/LCE ₄ | 81 | 87 | 7.19 | 739 | 354 | 397 |
| 0.5-SBA-15/LCE ₄ | 92 | 101 | 11.22 | 1113 | 346 | 396 |
| 1.0-SBA-15/LCE ₄ | 90 | 100 | 10.12 | 1007 | 350 | 399 |
| 1.5-SBA-15/LCE ₄ | 86 | 94 | 9.81 | 991 | 351 | 398 |
| 2.0-SBA-15/LCE ₄ | 84 | 93 | 7.96 | 806 | 348 | 397 |

low addition, the homogeneous dispersion of SBA-15 and LCE_4 enhanced the interaction force between inorganic and organic phases, which further improved the T_g . Unfortunately, when the additional amount of SBA-15 exceeded 1.0 wt%, a slight agglomeration phenomenon occurred between SBA-15 and LCE_4 , weakening the interaction force between the inorganic and organic phases, which results in a decrease in T_g .

$$E'r = 3v_rRT_r \quad (1)$$

where $E'r$ represents the rubber platform modulus at $T_g + 30$ °C, R represents the gas mole constant, T_r represents the Kelvin temperature at $T_g + 30$ °C.

The thermal decomposition behavior of LCE_4 and SBA-15/ LCE_4 composites was compared by TGA in the temperature range of 50–800 °C. The specific data are given in Fig. 11 and Table 3. It could be seen from the figure that LCE_4 and the composites degraded through one step, indicating that there was a good phase connection between mesoporous SBA-15 and LCE_4 matrix, and KH560 was successfully grafted to the surface of mesoporous SBA-15 and that water and other volatile substances were not present in the composite [57, 58]. It can be seen from Table 3 that with the gradual increase in the addition of mesoporous SBA-15, the thermal decomposition temperatures of the composites in $T_{10\%}$ and $T_{50\%}$ were significantly increased compared with that of pure LCE_4 , which proved that the addition of mesoporous SBA-15 into LCE_4 could improve the thermal stability of composites. The improvement of thermal stability

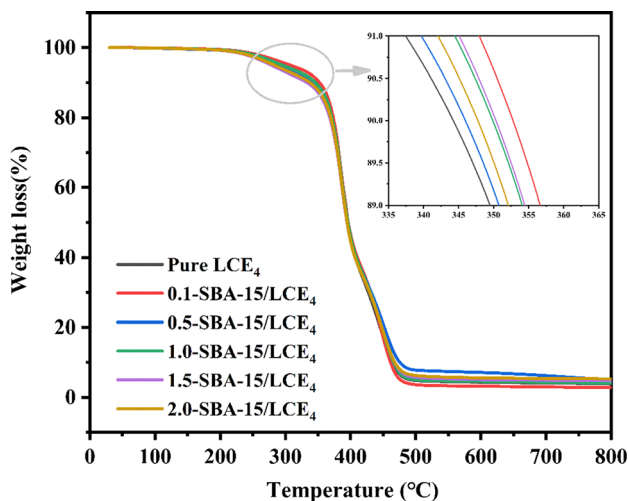


Figure 11 TGA diagram of pure LCE_4 and SBA-15/ LCE_4 composites.

could be attributed to the good thermal stability of LCE_4 and mesoporous SBA-15. In addition, the most critical factor was that LCE_4 and the modified mesoporous SBA-15 form a close cross-linking network under the action of a curing agent, which enhanced the interaction.

Figure 12 shows the mechanical properties of the prepared LCE_4 and SBA-15/ LCE_4 composites, including tensile strength (Fig. 12a), tensile modulus (Fig. 12b), elongation at break (Fig. 12c), and stress–strain curves (Fig. 12d); the specific values are shown in Table 4. Interestingly, it can be seen from Fig. 12a that as the mass fraction of mesoporous SBA-15 increased from 0 wt% (49.35 MPa) to 0.5 wt% (55.44 MPa), the tensile strength of the SBA-15/ LCE_4 composite increased. However, with the gradual increase of mesoporous SBA-15 content of 1.0 wt% (51.62 MPa), 1.5 wt% (50.63 MPa), 2.0 wt% (49.17 MPa), the tensile strength of SBA-15/ LCE_4 composites decreased. This phenomenon originated from the strong interaction between mesoporous SBA-15 and LCE_4 evenly dispersed on the one hand and with the appropriate affinity and chemical interaction between SBA-15 and LCE_4 on the other hand. Compared with the 0.5-SBA-15/ LCE_4 composites, the tensile strength decreased when the addition amount was 1.0 wt%, 1.5 wt%, and 2.0 wt%, which could be attributed to the slight agglomeration phenomenon in the mesopore SBA-15 of LCE_4 matrix with the increase of the addition amount of mesopore SBA-15. Most importantly, the elongation at break of the 0.5-SBA-15/ LCE_4 composite was 5.07%, increasing 33.1% compared with pure LCE_4 .

Conclusions

In this work, a LCE_4 consisting of flexible chain and rigid mesogenic units was prepared and thermally cured by MHHPA. The mechanism of the curing reaction and the liquid crystal phase structure was studied. The results showed that with the progress of the cross-linking and curing reaction, a nematic liquid crystal with a “schlieren-like” structure was observed, and the microdomain density of the liquid crystal gradually increased. Due to the introduction of mesogenic elements, the dielectric constant and dielectric loss of the prepared LCE_4 /MHHPA samples were as low as 3.25 and 0.036, which were significantly better than ordinary epoxy resins. Even

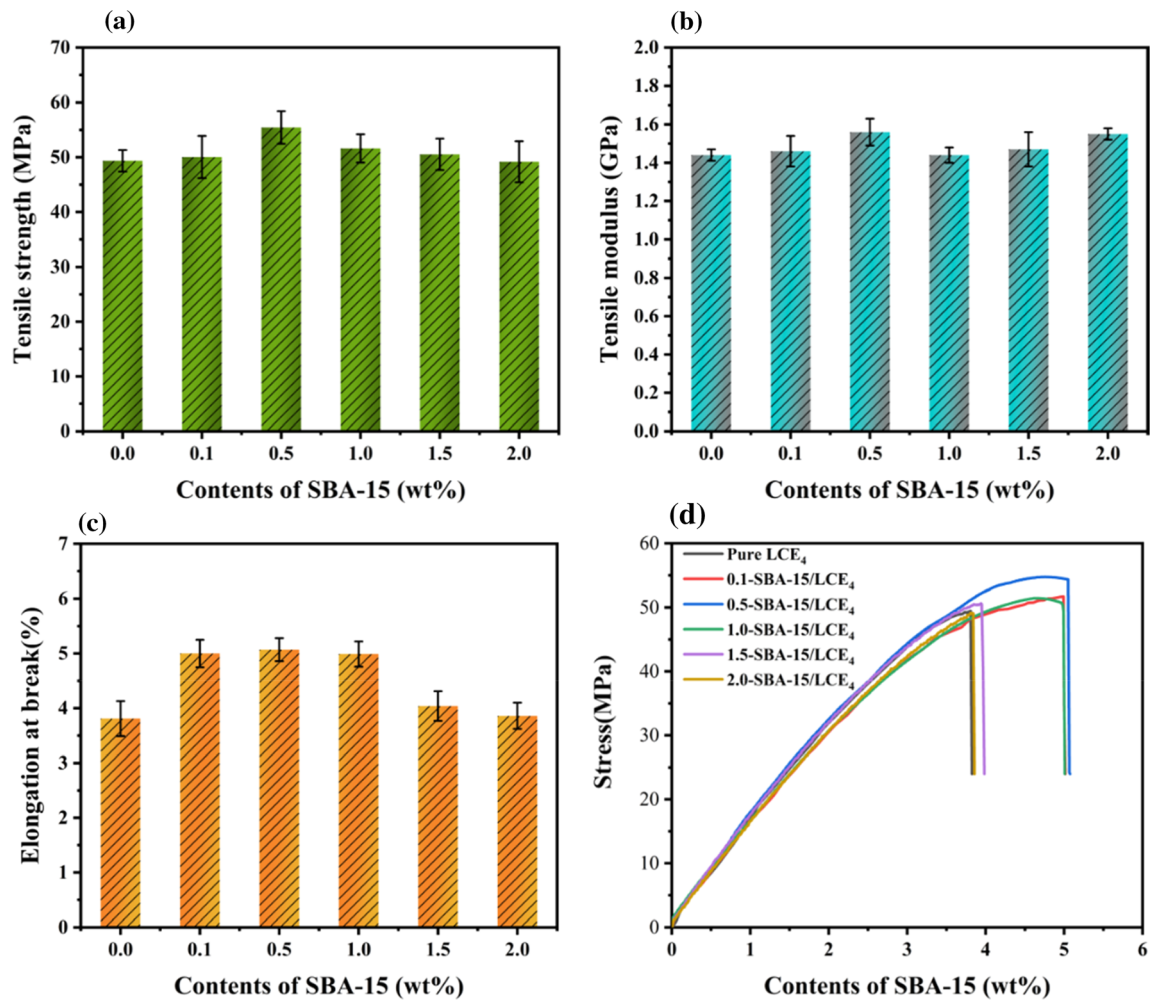


Figure 12 The tensile strength of SBA-15/LCE₄ composites **a**; the tensile modulus parameter of SBA-15/LCE₄ composites **b**; the elongation at break of SBA-15/LCE₄ composites **c**; SBA-15/LCE₄ composite of stress–strain curve **d**.

Table 4 Mechanical properties of LCE₄ and SBA-15/LCE₄ composite materials

| Sample | Tensile strength (MPa) | Tensile modulus (GPa) | Elongation at break (%) |
|-----------------------------|------------------------|-----------------------|-------------------------|
| Pure LCE ₄ | 49.35 ± 1.97 | 1.44 ± 0.03 | 3.81 ± 0.32 |
| 0.1-SBA-15/LCE ₄ | 50.05 ± 3.86 | 1.46 ± 0.08 | 5.00 ± 0.25 |
| 0.5-SBA-15/LCE ₄ | 55.44 ± 2.98 | 1.56 ± 0.07 | 5.07 ± 0.21 |
| 1.0-SBA-15/LCE ₄ | 51.62 ± 2.59 | 1.44 ± 0.04 | 4.99 ± 0.23 |
| 1.5-SBA-15/LCE ₄ | 50.63 ± 2.88 | 1.47 ± 0.09 | 3.97 ± 0.27 |
| 2.0-SBA-15/LCE ₄ | 49.17 ± 4.41 | 1.55 ± 0.03 | 3.86 ± 0.24 |

compared with the liquid crystal epoxy resin systems studied by Zhang et al. [24], Liu et al. [25], Guo et al. [59], they all have different degrees of reduction. Secondly, the mesoporous SBA-15 was surface-functionalized with KH560, and then, it was used as a low-dielectric hydrophobic filler uniformly dispersed in the liquid crystal epoxy resin to prepare the corresponding SBA-15/LCE₄ composites. The results

showed that KH560 successfully modified the surface of mesoporous SBA-15, and the composites exhibited better dielectric, thermal, mechanical, and hydrophobic properties than pure LCE₄. Specifically, when the additional amount of mesopore SBA-15 was 0.5 wt%, the dielectric constant and dielectric loss of the composites were 2.35 and 0.025, which decreased 24.7% and 31%, respectively, compared

with pure LCE₄. The T_g of the composite was 101 °C, which was 16 °C higher of pure LCE₄. In addition, the introduction of mesoporous SBA-15 made the hydrophobicity, thermal stability, and mechanical properties of the composites significantly improved compared with pure LCE₄, which makes it have a broad application prospect in electronic packaging, electrical, and electronic fields.

Acknowledgements

The study was supported by the Guangzhou Science and Technology Program Key Projects (No. 201904010244). The authors would like to thank Huang Zhenyun from shiyanjia laboratory for support of DSC and BET analysis (www.Shiyanjia.com).

Data availability

The raw/processed data required to reproduce these findings cannot be shared at this time as the data also form part of an ongoing study.

Declarations

Conflict of interest The authors declare that they have no known competing financial interests or personal relationships that could have appeared to influence the work reported in this paper.

References

- [1] Feng CP, Chen L, Wei F, Ni HY, Chen J, Yang W (2016) Highly thermally conductive UHMWPE/graphite composites with segregated structures. *RSC Adv* 6(70):65709–65713
- [2] Kim K, Kim M, Kim J (2014) Thermal and mechanical properties of epoxy composites with a binary particle filler system consisting of aggregated and whisker type boron nitride particles. *Compos Sci Technol* 103:72–77
- [3] Luo T, Lloyd JR (2012) Enhancement of thermal energy transport across graphene/graphite and polymer interfaces: a molecular dynamics study. *Adv Func Mater* 22(12):2495–2502
- [4] Hopkins PE, Baraket M, Barnat EV, Beechem TE, Kearney SP, Duda JC, Robinson JT, Walton SG (2012) Manipulating thermal conductance at metal-graphene contacts via chemical functionalization. *Nano Lett* 12(2):590–595
- [5] Taha-Tijerina J, Narayanan TN, Gao G, Rohde M, Tsentelovich DA, Pasquali M, Ajayan PM (2012) Electrically insulating thermal nano-oils using 2D fillers. *ACS Nano* 6(2):1214–1220
- [6] Liu Y, Qian C, Qu L, Wu Y, Zhang Y, Wu X, Zou B, Chen W, Chen Z, Chi Z, Liu S, Chen X, Xu J (2015) A bulk dielectric polymer film with intrinsic ultralow dielectric constant and outstanding comprehensive properties. *Chem Mater* 27(19):6543–6549
- [7] Huang X, Iizuka T, Jiang P, Ohki Y, Tanaka T (2012) Role of interface on the thermal conductivity of highly filled dielectric epoxy/AlN composites. *J Phys Chem C* 116(25):13629–13639
- [8] Jiang Q, Zhang W, Hao J, Wei Y, Mu J, Jiang Z (2015) A unique “cage-cage” shaped hydrophobic fluoropolymer film derived from a novel double-decker structural POSS with a low dielectric constant.” *J Mater Chem C* 3(44):11729–11734
- [9] Tousignant MN, Rice NA, Niskanen J, Richard CM, Ritaine D, Adronov A, Lessard BH (2021) High performance organic electronic devices based on a green hybrid dielectric. *Adv Electron Mater.* <https://doi.org/10.1002/aelm.202100700>
- [10] Wu B, Liu H, Fu R, Song X, Su X, Liu X (2021) Epoxy-matrix composite with low dielectric constant and high thermal conductivity fabricated by HGMs/Al₂O₃ co-continuous skeleton. *J Alloys Compd* 869:159332. <https://doi.org/10.1016/j.jallcom.2021.159332>
- [11] Xu X, Hu R, Chen M, Dong J, Xiao B, Wang Q, Wang H (2020) 3D boron nitride foam filled epoxy composites with significantly enhanced thermal conductivity by a facial and scalable approach. *Chem Eng J* 397:125447. <https://doi.org/10.1016/j.cej.2020.125447>
- [12] Zhang P, Zhao J, Zhang K, Bai R, Wang Y, Hua C, Wu Y, Liu X, Xu H, Li Y (2016) Fluorographene/polyimide composite films: Mechanical, electrical, hydrophobic, thermal and low dielectric properties. *Compos Part a-Appl Sci Manuf* 84:428–434
- [13] Wahab MA, Chaobin H, Altalhi T, Albaqami MD, Alotman ZA, Haque R (2021) Nanopore engineered tortuosity towards thermo-mechanically enhanced low-k polymer-mesoporous organosilica composite membranes. *Compos Sci Technol* 211:108854. <https://doi.org/10.1016/j.compscitech.2021.108854>
- [14] Wang L, Bai Z, Liu C, Wei R, Liu X (2021) Porous fluorinated polyarylene ether nitrile as ultralow permittivity dielectrics used under humid environment. *J Mater Chem C* 9(3):860–868
- [15] Liu X, Yue D, Yang C, Li N, Gao S, Liu Y, Mo G, Wu Z, Yin J, Su B, Li L (2019) Fluorinated carbon nanofiber/polyimide composites: Electrical, mechanical, and hydrophobic properties. *Surf Coat Technol* 361:206–211

- [16] Yu Z, Wu S, Li C, Xiao Y, Zheng L, Liu J, Zhang B (2021) Ultra-low dielectric constant fluorinated graphene/polybenzoxazole composite films with excellent thermal stabilities and mechanical properties. *Compos Part a-Appl Sci Manuf* 145:106387. <https://doi.org/10.1016/j.compositesa.2021.106387>
- [17] Chrusciel JJ, Lesniak E (2015) Modification of epoxy resins with functional silanes, polysiloxanes, silsesquioxanes, silica and silicates. *Prog Polym Sci* 41:67–121
- [18] Pan Y-T, Zhang L, Zhao X, Wang D-Y (2017) Interfacial engineering of renewable metal organic framework derived honeycomb-like nanoporous aluminum hydroxide with tunable porosity. *Chem Sci* 8(5):3399–3409
- [19] Jiang S-D, Tang G, Chen J, Huang Z-Q, Hu Y (2018) Bio-based polyelectrolyte multilayer-coated hollow mesoporous silica as a green flame retardant for epoxy resin. *J Hazard Mater* 342:689–697
- [20] Xu Y-J, Wang J, Tan Y, Qi M, Chen L, Wang Y-Z (2018) A novel and feasible approach for one-pack flame-retardant epoxy resin with long pot life and fast curing. *Chem Eng J* 337:30–39
- [21] Guo H, Lu M, Liang L, Wu K, Ma D, Xue W (2017) Liquid crystalline epoxies with lateral substituents showing a low dielectric constant and high thermal conductivity. *J Electron Mater* 46(2):982–991. <https://doi.org/10.1007/s11664-016-5003-6>
- [22] Carfagna C, Amendola E, Giamberini M (1994) Rigid-rod networks - liquid-crystalline epoxy-resins. *Compos Struct* 27(1–2):37–43
- [23] Li Y, Badrinarayanan P, Kessler MR (2013) Liquid crystalline epoxy resin based on biphenyl mesogen: Thermal characterization. *Polymer* 54(12):3017–3025
- [24] Zhang X, Gu A, Liang G, Zhuo D, Yuan L (2011) Liquid crystalline epoxy resin modified cyanate ester for high performance electronic packaging. *J Polym Res* 18(6):1441–1450
- [25] Liu Z, Yuan L, Liang G, Gu A (2015) Tough epoxy/cyanate ester resins with improved thermal stability, lower dielectric constant and loss based on unique hyperbranched polysiloxane liquid crystalline. *Polym Adv Technol* 26(12):1608–1618
- [26] Y Li, V Ambroggi, P Cerruti, M Goswami, Z Yang, MR Kessler, O Rios (2021) Functional liquid crystalline epoxy networks and composites: from materials design to applications. *Int Mater Rev*
- [27] Yang X, Zhong X, Zhang J, Gu J (2021) Intrinsic high thermal conductive liquid crystal epoxy film simultaneously combining with excellent intrinsic self-healing performance. *J Mater Sci Technol* 68:209–215
- [28] Hong Y, Goh M (2021) Advances in liquid crystalline epoxy resins for high thermal conductivity. *Polymers* 13(8):1302. <https://doi.org/10.3390/polym13081302>
- [29] Tian K, Yang S, Niu J, Wang H (2021) Enhanced thermal conductivity and mechanical toughness of the epoxy resin by incorporation of mesogens without nanofillers. *Ieee Access* 9:31575–31580
- [30] Kim Y, Yoo S, Lee HG, Won Y, Choi J, Kang K (2021) Structural analysis of silica aerogels for the interlayer dielectric in semiconductor devices. *Ceram Int* 47(21):29722–29729
- [31] Nam J-Y, Kim H-K, Song Y-S (2021) Fabrication and analysis of sepiolite/glass microcapsules/liquid crystal polymer composites. *Molecules* 26(9):2522. <https://doi.org/10.3390/molecules26092522>
- [32] Shwaykani H, El-Hajj A, Costantine J, Al-Husseini M (2021) A calibration-free method for the dielectric constant calculation of low-loss materials. *Ieee Trans Instrum Meas* 70:1–10. <https://doi.org/10.1109/TIM.2020.3011765>
- [33] Zhang J, Xu R, Yu D (2007) A novel poly-benzoxazinyll functionalized polyhedral oligomeric silsesquioxane and its nanocomposite with polybenzoxazine. *Eur Polymer J* 43(3):743–752
- [34] Du W, Shan J, Wu Y, Xu R, Yu D (2010) Preparation and characterization of polybenzoxazine/trisilanol polyhedral oligomeric silsesquioxanes composites. *Mater Des* 31(4):1720–1725
- [35] Yang PD, Zhao DY, Margolese DI, Chmelka BF, Stucky GD (1998) Generalized syntheses of large-pore mesoporous metal oxides with semicrystalline frameworks. *Nature* 396(6707):152–155
- [36] Park I, Peng HG, Gidley DW, Xue SQ, Pinnavaia TJ (2006) Epoxy-silica mesocomposites with enhanced tensile properties and oxygen permeability. *Chem Mater* 18(3):650–656
- [37] Lin J, Wang X (2008) Preparation, microstructure, and properties of novel low-kappa brominated epoxy/mesoporous silica composites. *Eur Polymer J* 44(5):1414–1427
- [38] Purushothaman R (2015) Amine functionalized SBA-15/terpolyimide composites with low dielectric constant. *J Porous Mater* 22(3):585–594
- [39] Hukkamaki J, Suvanto S, Suvanto M, Pakkanen TT (2004) Influence of the pore structure of MCM-41 and SBA-15 silica fibers on atomic layer chemical vapor deposition of Cobalt carbonyl. *Langmuir* 20(23):10288–10295
- [40] Yao J, Sheng M, Bai S, Su H, Shang H, Deng H, Sun J (2021) Ionic Liquids grafted mesoporous silica for chemical fixation of CO₂ to cyclic carbonate: morphology effect. *Catal Lett*. <https://doi.org/10.1007/s10562-021-03667-9>
- [41] Lu Y, Lin Q, Ren W, Zhang Y (2015) Investigation on the preparation and properties of low-dielectric ethylene-vinyl

- acetate rubber/mesoporous silica composites. *J Polym Res* 22(4). <https://doi.org/10.1007/s10965-015-0694-6>
- [42] Lasmi S, Zoukrami F, Antonio Marcos-Fernandez A, Guerba H (2020) Influence of modified mesoporous silica SBA-15 and compatibilizer on the properties and structure of ethylene-vinyl acetate copolymer-based nanocomposites. *Polym-Plast Technol Mater* 59(18):2003–2017
- [43] Jahromi S, Kuipers WAG, Norder B, Mijs WJ (1995) Liquid-crystalline epoxide thermosets - dynamic-mechanical and thermal-properties. *Macromolecules* 28(7):2201–2211
- [44] Mormann W, Broche M, Schwarz P (1997) Mesogenic azomethine based diepoxides - monomers for the synthesis of “liquid crystal” thermoset networks. *Macromol Chem Phys* 198(11):3615–3626
- [45] Lee JY, Jang JS (1998) Effect of substituents on the curing of liquid crystalline epoxy resin. *J Polym Sci Part a-Polym Chem* 36(6):911–917
- [46] Ortiz C, Wagner M, Bhargava N, Ober CK, Kramer EJ (1998) Deformation of a polydomain, smectic liquid crystalline elastomer. *Macromolecules* 31(24):8531–8539
- [47] Shiota A, Ober CK (1998) Smectic networks obtained from twin LC epoxy monomers - Mechanical deformation of the smectic networks. *J Polym Sci Part B-Polym Phys* 36(1):31–38
- [48] Ribera D, Mantecon A, Serra A (2001) Synthesis and crosslinking of a series of dimeric liquid crystalline epoxy resins containing imine mesogens. *Macromol Chem Phys* 202(9):1658–1671
- [49] Zhang Q, Chen G, Wu K, Shi J, Liang L, Lu M (2020) Biphenyl liquid crystal epoxy containing flexible chain: Synthesis and thermal properties. *J Appl Polym Sci* 137(38):49143. <https://doi.org/10.1002/app.49143>
- [50] Luo T, Wei X, Luo S, Li H, Li W (2013) Study of Surface Modification of Al₂O₃ Nanoparticles with KH-560. *Asian J Chem* 25(12):6777–6779
- [51] Zheng W, Tang C, Xie J, Gui Y (2019) Micro-scale effects of nano-SiO₂ modification with silane coupling agents on the cellulose/nano-SiO₂ interface. *Nanotechnology* 30(44):445701. <https://doi.org/10.1088/1361-6528/ab3546>
- [52] Kruk M, Jaroniec M (2001) Gas adsorption characterization of ordered organic-inorganic nanocomposite materials. *Chem Mater* 13(10):3169–3183
- [53] Ma J, Liu Q, Chen D, Wen S, Wang T (2015) Synthesis and characterisation of pore-expanded mesoporous silica materials. *Micro Nano Letters* 10(2):140–144
- [54] Luo P, Xu M, Wang S, Xu Y (2017) Structural Dynamic Mechanical and Dielectric Properties of Mesoporous Silica/Epoxy Resin Nanocomposites. *Ieee Trans Dielectr Electr Insul* 24(3):1685–1697
- [55] Jin C, Lin S, Wetzel JT (2001) Evaluation of ultra-low-k dielectric materials for advanced interconnects. *J Electron Mater* 30(4):284–289
- [56] Zhao X-Y, Liu H-J (2010) Review of polymer materials with low dielectric constant. *Polym Int* 59(5):597–606
- [57] Lin J, Wang X (2008) New type of low-dielectric composites based on o-cresol novolac epoxy resin and mesoporous silicas: fabrication and performances. *J Mater Sci* 43(13):4455–4465. <https://doi.org/10.1177/0954008313511347>
- [58] Prabunathan P, Sethuraman K, Alagar M (2014) Development of bio-based F-SBA-15 reinforced epoxy nanocomposites for low-k dielectric applications. *High Perform Polym* 26(3):283–289
- [59] Guo H, Zheng J, Gan J, Liang L, Wu K, Lu M (2015) Relationship between crosslinking structure and low dielectric constant of hydrophobic epoxies based on substituted biphenyl mesogenic units. *RSC Adv* 5(107):88014–88020

Publisher's Note Springer Nature remains neutral with regard to jurisdictional claims in published maps and institutional affiliations.